Nat. Hazards Earth Syst. Sci. Discuss., 1, 3553–3575, 2013
www.nat-hazards-earth-syst-sci-discuss.net/1/3553/2013/
doi:10.5194/nhessd-1-3553-2013

Natural Hazards and Earth System Sciences
Discussions
Open Access

Comment on "Comparative study on earthquake and ground based transmitter induced radiation belt electron precipitation at middle latitude" by Sideropoulos et al. (2011)

J.-A. Sauvaud[1], M. Parrot[2], and E. Slominska[3]

[1]IRAP-UMR5277, CNRS – University of Toulouse, Toulouse, France
[2]LPC2E-UMR7328, CNRS – University of Orléans, Orléans, France
[3]Space Research Center (CBK), Academy of Sciences, Warsaw, Poland

Received: 19 June 2013 – Accepted: 3 July 2013 – Published: 26 July 2013

Correspondence to: J.-A. Sauvaud (jsauvaud@irap.omp.eu)

Published by Copernicus Publications on behalf of the European Geosciences Union.

Abstract

We show that many, if not all, electron bursts claimed to be earthquake precursors by Sideropoulos et al. (2011) are due to the cyclotron resonance of electrons with monochromatic waves from VLF transmitters. The geographic distribution of the VLF-related electron bursts is established during a period in 2007, when the powerful NWC transmitter is off.

1 Introduction

Recently a number of papers have appeared in the literature claiming that earthquake are preceded by the detection of electron bursts onboard the low altitude sun-synchronous satellite Demeter. Several of these papers present case studies and include some statistics (e.g., Sideropoulos et al., 2011; Anagnostopoulos et al., 2012) while others are based only on statistical studies (e.g., Zhang et al., 2010, 2013). While case studies allow a careful examination of the presented results, statistical studies are almost immune to examination of the initial data allowing the authors to claim for earthquake precursor using energetic particle data.

The aim of this comment is to show that many, if not all, electron bursts measured onboard Demeter and presented as earthquake precursor by Sideropoulos et al. (2011) result from the cyclotron resonance of radiation belt electrons with monochromatic VLF waves emitted by powerful VLF transmitters. The paper is divided in two parts. In the first part we will examine bursts presented as examples of earthquake precursors when the NWC transmitter (North West Cape) in Australia is switched on. In the second part we will examine a published case pertaining to periods when NWC is switched off, i.e., from 1 July 2007 to 22 January 2008. During that period, geographical distributions of VLF transmitters and of the induced electron bursts are presented and modeled.

NHESSD

1, 3553–3575, 2013

This study shows that the measured electron bursts are not associated with earthquake but with cyclotron resonance of electrons with monochromatic waves emitted by VLF transmitters.

2 NWC on

In a recent paper, Sideropoulos et al. (2011) studied 4 cases of Demeter data showing electron bursts when the NWC transmitter was operating. NWC, located in the North West Cape of Australia, emits a power of 1 MW at 19.8 kHz. The effect of this transmitter on energetic radiation belt electrons measured onboard the low-orbiting polar spacecraft DEMETER was reported by Sauvaud et al. (2008) and Gamble et al. (2008). More recently, a paper by Selesnick et al. (2013) provides a full simulation of the effect of the NWC waves on the radiation belt electrons based on a stochastic model of electron transport that includes pitch angle diffusion, radial diffusion, energy loss, and azimuthal drift.

The main signature of the interaction of energetic electron with the transmitter monochromatic waves as seen at 700 km altitude is the formation of a wisp features (Sauvaud et al., 2008; Gamble et al., 2008). The enhancements are initially observed within a few degrees west of NWC and are present in 95 % of the orbital data east of the transmitter up to the South Atlantic Anomaly for time periods when the transmitter is broadcasting and located in nightside.

Studying electron bursts, Sideropoulos et al. (2011) did not take advantage of the fine energy resolution of the IDP energetic electron instrument onboard Demeter (see Sauvaud et al., 2006, 2013) and reach conclusions on electron burst based only on the examination of the variations along the Demeter orbit of 3 integral fluxes in the energy bands: 72–526, 526–971 and 971–2350 keV. However the energy dispersed electron structure caused by NWC is only clearly apparent in the energy-time spectrograms of the IDP instruments with 128 (256) energy channels in survey (burst) mode. In Fig. 1 we show such measurements, for 2 cases studied by Sideropoulos, together

NHESSD
1, 3553–3575, 2013

with the electric component of waves in the frequency range from 10 kHz to 20 kHz provided by the ICE instrument onboard Demeter and with the three integral energy fluxes discussed above (note that the energy range 72–90 keV which is affected by electronic noise has been excluded). Figure 1 should be compared with Figs. 1a and 2a of Sideropoulos et al. (2011).

Figure 1a presents measurements for which the electron bursts detected around 14:30 and 14:53 UT on 2 November 2006 have been attributed by Sideropoulos et al. (2011) to the near-equatorial resonance of electrons with the waves emitted by the NWC transmitter. The energy-time spectrogram of electrons presented in Fig. 1a indeed shows at 14:30 UT the typical energy dispersed structure expected for such resonance, here in the Southern Hemisphere. Later during the same half-orbit, around 14:53 UT, the measurements are made slightly westward of the NWC transmitter, which results in a less marked structure.

Figure 1b presents similar measurement performed over Australia on east of NWC on 13 August 2005 between 12:53 and 13:29 UT, during a pass considered as earthquake related by Sideropoulos et al. (2011). Demeter encounters indeed electron bursts two times, at conjugate locations in the Northern and Southern Hemispheres, around 13:01 UT and 13:20 UT. It must be stressed the energy dispersion nature of the bursts is clearly visible in Fig. 1b and they are very similar to the structures displayed in Fig. 1a. However, Sideropoulos et al. attributed these bursts to a “clear example” of precursor of an earthquake occurring on 16 August 2005 in Japan. They associated the electron burst with the enhanced VLF signal recorded in the Northern Hemisphere between 13:17 and 13:25 UT and noted that another VLF burst were also seen in the Southern Hemisphere. Two main remarks must be done regarding this association: (i) the considered VLF waves being largely distributed in frequency they should resonate with electrons in a broad range of energies, which is clearly not observed, and (ii) the power of the natural VLF waves is weak compared to the NWC signal. In order to illustrate this fact, Fig. 2 presents the nightside distribution of the VLF waves in a frequency range 15–25 kHz in the vicinity of Australia and in the conjugate hemisphere.

NHESSD
1, 3553–3575, 2013

Just above NWC the average wave power is higher than $10^4\,\mu V^2\,m^{-2}\,s^{-1}$, while the power of the natural VLF waves recorded onboard Demeter around 13:20 UT is less than $10^1\,\mu V^2\,cm^{-2}\,s^{-1}$. The effect of NWC is thus expected to be completely dominant.

Furthermore, the electron bursts, when displayed in an energy-time spectrogram, show the typical dispersion structure resulting from their interaction with monochromatic waves (Fig. 3). Recently, Selesnick et al. (2013) performed a full simulation of the effect of the NWC waves on the radiation belt electrons based on a stochastic model of electron transport that includes pitch angle diffusion, radial diffusion, energy loss, and azimuthal drift. They showed that the Demeter electron dispersed structures are in agreement with their calculations.

More simply, we can compute the energy of resonant electrons with 19.8 kHz waves. The results are given in Fig. 3 where we display the electron dispersed structure measured at around 13:20 UT on 13 August 2005, together with the energy change expected from a simple model of equatorial cyclotron resonance (see Koons et al., 1981).

Whistler-modes waves from NWC are at fixed frequency, ω, with the index of refraction $\mu = kc/\omega$ given by:

$$\mu^2 = 1 + \frac{\omega_p^2}{\omega(\Omega|\cos\theta| - \omega)} \tag{1}$$

For wave number k, wave normal angle θ, plasma frequency ω_p, and electron cyclotron frequency Ω. The condition for electron-wave cyclotron resonance is

$$\omega - k_{\|}v_{\|} = \frac{n\Omega}{\gamma} \tag{2}$$

Where n is a positive or negative integer, or zero, $k_{\|} = k\cos\theta$, $v_{\|} = v\cos\alpha$, v is the electron speed, γ the Lorentz factor, and α is the local pitch angle. The wave normal is taken equal to 60° (Selesnick et al., 2013). For equatorial resonance, the pitch-angle of electrons is computed in a way that electron have a 90° pitch angle at the satellite

NHESSD
1, 3553–3575, 2013

altitude. Following Selesnick et al. (2013), for evaluation of the plasma frequency, the plasma density is taken equal to $A \times 10^3 L^{-1} + 10^6 \exp(-h/350)\,\mathrm{cm}^{-3}$, with A varying in the range 9000–18 000 cm^{-3}. The two terms represent the plasmasphere and the ionosphere. Note that above $L = 1.4$ the ionospheric density represents only a weak part of the plasmaspheric one.

The results of the computations are displayed together with the measured electron energy spectrogram (Fig. 3). The computed energy resonance (white curves) well fit the measured electron dispersion shape. Here A term in the plasma density relation is taken equal to 18 000 cm^{-3} for the solid curve. The dashed curves are for a inner plasmasphere density 30 % higher and 30 % lower.

From the comparison of the shape and location of the energy structures and of the model energy band we conclude, following earlier works by Sauvaud et al. (2008), Gamble et al. (2008) and Selesnick et al. (2013) that the observed "electron burst" are due to the resonance of electrons of the inner radiation belt drift with the monochromatic waves emitted by the NWC transmitter. The electrons are then eastward drifting and can hardly be interpreted as due to a hypothetical precursor of the Japan earthquake occurring days after the observations.

Figure 4a and b presents two more cases of Demeter measurements close to the Australian NWC meridian on 12 May 2006 and 16 May 2006. These figures must be compared to Fig. 4a and b of Sideropoulos et al. (2011). The measurements performed onboard Demeter on 12 May 2006 (Fig. 4a) are similar to those presented in Fig. 1, the spacecraft passes eastward of NWC i.e. in a region where the electrons drift, and the same interpretation applies there.

As stated in Sideropoulos et al. (2011), Fig. 4b shows no electron burst around 09:25 UT. At NWC, the sunset is at 17:50 LT, which corresponds to 09:50 UT. At 09:25, NWC is still in the day and the waves are strongly attenuated by the ionosphere (Cohen and Inan, 2012). It is thus expected that no clear electron structure resulting from wave-particle interaction can be detected. Later, when the spacecraft reach the conjugate hemisphere a very weak structure can be seen in Fig. 4b around 09:43 UT in the

NHESSD
1, 3553–3575, 2013

energy-time electron spectrogram for energies in the range 200–300 keV. The transmitter is now in penumbra and a weak part of the wave power escapes the ionosphere and interacts with electrons.

To conclude this part, the absence of well-marked energy dispersed structure is here due to the local time of the NWC station and cannot be attributed to the fact that "electron precipitation activity ceases a few hours before a great earthquake" as stated in Sideropoulos et al. (2011).

3 NWC off

Sideropoulos et al. (2011) also studied electron burst when the NWC transmitter is off. They presented a case (their Fig. 3) obtained on 18 September 2006 where two electron burst can be detected.

Figure 5 gives the Demeter measurements during that period in the same format as in Figs. 1 and 4. A slightly dispersed electron dispersed structure is clearly seen at low energies around 13:14–13:15 UT. A conjugate enhancement of electron fluxes is seen at the lowest energies around 12:53–12:54 UT. Such electron flux enhancements are quite common during the period when NWC was off, i.e. between 1 July 2007 and 22 January 2008. Before to claim for an earthquake cause for such measurements, one has to check if these bursts can be produced from the interaction of electrons with other VLF transmitters.

The geographic distribution of VLF transmitter is given in Figs. 6–8. Table 1 provides the transmitters code, frequency and geographical position. Figure 6 displays the power distribution measured at Demeter altitude between 15 and 25 kHz (see Parrot et al., 2012). In Fig. 6 the black lines indicate the $L = 2$ contours in the Northern and Southern Hemisphere. In the US sector, four main transmitters are operating: NPM at very low latitude, NLK, NML and NAA at L values somewhat higher than 2. The emitted waves can be seen in the Southern Hemisphere around $L = 2$. It means that if electrons are resonating with these transmitters the energy-dispersed structures should be detected

NHESSD
1, 3553–3575, 2013

at L value on the order of 2. In Europa three main transmitters are detected, GQD in UK, HWU in France and DHO in Germany, the corresponding waves are detected southward of South Africa around $L = 2$. In the Asian sector three transmitters are detected, in the Southern Hemisphere NWC at $L = 1.4$ and NTS at L slightly higher than 2. In the Northern Hemisphere: UBE at L equal to 2 is confused with the conjugate waves of NTS. Except NWC, all the transmitters were operating during the period when the data presented in Fig. 5 were obtained.

Furthermore other navigation transmitters are working at lower frequencies. Figure 7 gives the position of 3 ALFA transmitters in Russia, which emit sequentially at 11.8 kHz, 12.6 kHz and 14.8 kHz. Figure 8 provides measurements at higher frequencies, between 25 and 60 kHz. Here 13 more transmitters are clearly identified. Two of them are located just below $L = 1.5$, NAU (US) and NSC (Italy), with their conjugate area around $L = 1.5$. Note that in Figs. 6 and 8 the frequency resolution is only 3.2 kHz, which leads to a large underestimation of the measured power of the transmitters.

The result of a search of dispersed electron structure during a three-month period from July to September 2007, when NWC was off, is presented in Fig. 9. The upper panel shows the distribution of the electron bursts in a UT-longitude diagram. As expected from the sun-synchronous orbit of Demeter the bursts are found along straight lines resulting from the rotation of the Earth below the satellite. UT is always UT = 10-long/15 and UT = 22-long/15. Red symbols are for measurements made near 10:00 LT and black ones for measurements made near 22:00 LT. The black (red) double traces correspond to nightside (dayside) passes of the spacecraft crossing first a northern (southern) structure and about one hour later the conjugate structure in the Southern (Northern) Hemisphere, after flying over the dayside (nightside) part of the Earth. Single traces correspond to structures with no conjugate. The structures are thus well organized in a UT-longitude space indicating of a probable geographic origin. The bottom panel of Fig. 8 gives the latitude-longitude distribution with superposed curves giving the $L = 2$ and $L = 1.5$ locations in the Northern and Southern Hemisphere. The structures are mainly grouped along $L = 2$ with two notable exceptions: in the US sector at

NHESSD
1, 3553–3575, 2013

longitudes from −100 to −70° and in the South-African sector at longitudes between 10 and 40° where they are located at lower L shells.

Let us supposed that each structure is resulting from the interaction of electrons with VLF waves emitted by human transmitters. For the waves to reach the magnetosphere, the station must be in darkness or at the beginning of the day, in order for the electron density in the D-region of the ionosphere not to be high enough to prevent the escape of VLF power inside the magnetosphere (Cohen and Inan, 2012). Taking this into account it becomes simple to find the origin of the structures. Their origins are indicated in the upper panel of Fig. 8. US stand for United States, EU for Europa. Russia and Asia are also indicated. There is no structures recorded over the Atlantic, this comes from the fact that there the electron drifting from the other part of the Earth are precipitating, due to the lowering of their mirror point in the Southern Hemisphere.

It is also remarkable that night side passes over Europa does not show electron structures while in the conjugate region there is a number of recorded electron structures. We attribute this to the weak field in the South-African sector, located on the East side of the South Atlantic Anomaly, where electrons resonating with the waves emitted by the European transmitter can be detected in the low B-field region at the satellite altitude. To illustrate this interpretation, we show in Fig. 10 a pass over South Africa where 3 successive electron bursts are recorded. The electron wisps are superposed with the energy changes expected from the resonance of inner belt electrons with waves emitted by European transmitters. The probable causes of the two structures at the highest L-shells are the French, HWU, and the Turkish transmitters, TBB, respectively emitting at 22.67 and 21.75 kHz, while the Italian NSY station broadcasting at 45.9 kHz causes the electron wisp at lower L-shell. Note in Fig. 10 that there is a similar low-latitude effect at a longitude of about −100° where the electron destabilized by the low-latitude NAU transmitter (40.8 kHz) are only detected in the Southern Hemisphere, in the west border of the South Atlantic Anomaly.

Finally Fig. 9 clearly shows that the location of the electron bursts (green symbols) detected as an earthquake precursor by Sideropoulos et al. (2011) are exactly

NHESSD
1, 3553–3575, 2013

superposed on the traces of electron bursts due to the cyclotron resonance of electrons with VLF transmitters.

4 Discussion and conclusion

We have presented evidences for the association of electron bursts recorded onboard Demeter with VLF waves of human origin. The powerful NWC transmitter has the most pronounced effects in the inner radiation belt electron population, as demonstrated in several papers (e.g. Sauvaud et al., 2008; Gamble et al., 2008; Li et al., 2011). Measurements made eastward of NWC, i.e. along the drift trajectory of electrons, should not be attributed to another cause without a very careful check of the transmitter expected effect. When this transmitter is in daylight, the absence of electron wisp should first be related with the absorption of the waves by the dayside ionosphere.

When the NWC transmitter is off, 20 more transmitters are still operating, with a clear effect to diffuse a part of the inner belt electrons in the drift loss cone. A statistical study of 3 months of data (≈ 1100 orbits) taken during such a period shows that the resulting electron bursts are worldwide distributed. Bursts, well fitted by electron-VLF wave resonance models, are indeed seen at all longitudes, except at those corresponding to the South Atlantic Anomaly.

A careful examination of the cases presented in Sideropoulos et al. (2011) as earthquake precursors thus indicate that all are due to the effect of VLF transmitters on the Earth's inner radiation belt. This result presented here shed some doubt on earthquake studies performed with the Demeter data without exploring the possibility that electron bursts could be linked with VLF transmitters (Anagnostopoulos et al., 2012; Zhang et al., 2010, 2013).

NHESSD
1, 3553–3575, 2013

The publication of this article
is financed by CNRS-INSU.

References

Anagnostopoulos, G. C., Vassiliadis, E., and Pulinets, S.: Characteristics of flux-time profiles, temporal evolution, and spatial distribution of radiation-belt electron precipitation bursts in the upper ionosphere before great and giant earthquakes, Ann. Geophys.-Italy, 55, 2012, doi:10.4401/ag-5365, 2011.

Cohen, M. B. and Inan, U. S.: Terrestrial VLF transmitter injection into the magnetosphere, J. Geophys. Res., 117, A08310, doi:10.1029/2012JA017992, 2012.

Cohen, M. B., Lehtien, N. G., and Inan, U. S.: Modems of ionospheric VLF absorption of powerful ground based transmitters, Geophys. Res. Lett., 39, L24101, doi:10.1029/2012GL054437, 2012.

Gamble, R. J., Rodger, C. J., Clilverd, M. A., Sauvaud, J. A., Thomson, N. R., Stewart, S. L., Mccormick, R. J., Parrot, M., and Berthelier, J.-J.: Radiation belt electron precipitation by man-made VLF transmissions, J. Geophys. Res., 113, A10211, doi:10.1029/2008JA013369, 2008.

Koons, H. C., Edgar, B. C., and Vampola, A. L.: Precipitation of inner zone electrons by whistler-mode waves from the VLF transmitters UMS and NW C. J. Geophys. Res., 86, 640–648, 1981.

Li, X., Yugian, M., Wang, P., Wang, H., Lu, H., Zhang, X., Huang, J., Shi, F., Yu, X., Xu, Y., Meng, X., Wang, H., Zhao, X., and Parrot, M.: Study of the North Wesp Cape electron belts observed by DEMETER satellite, J. Geophys. Res., 117, A04201, doi:10.1029/2011JA017121, 2012.

Sauvaud, J. A., Moreau, T., Maggiolo, R., Treilhou, J.-P., Jacquey, C., Cros, A., Coutelier, J., Rouzaud, J., Penou, E., and Gangloff, M.: High-energy electron detection onboard

NHESSD
1, 3553–3575, 2013

DEMETER: The IDP spectrometer, description and first results on the inner belt, Planet. Space. Sci., 54, 502–511, 2006.

Sauvaud, J.-A., Maggiolo, R., Jacquey, C., Parrot, M., Berthelier, J.-J., Gamble, R. J., and Rodger, C. J.: Radiation belt electron precipitation due to VLF transmitters: satellite observations, Geophys. Res. Lett., 35, L09101, doi:10.1029/2008GL033194, 2008.

Sauvaud, J.-A., Walt, M., Delcourt, D., Benoist, C., Penou, E., Chen, Y., Russell, C. T.: Inner radiation belt particle acceleration and energy structuring by drift resonance with ULF waves during geomagnetic storms, J. Geophys. Res., 118, 1723–1736, doi:10.1002/jgra.50125, 2013.

Selesnick, R. S., Albert, J. M., and Starks, M. J.: Influence of ground-based VLF radio transmitter on the inner electron radiation belt, J. Geophys. Res., 118, 628–635, doi:10.1002/jgra.50095, 2013.

Sidiropoulos, N. F., Anagnostopoulos, G., and Rigas, V.: Comparative study on earthquake and ground based transmitter induced radiation belt electron precipitation at middle latitudes, Nat. Hazards Earth Syst. Sci., 11, 1901–1913, doi:10.5194/nhess-11-1901-2011, 2011.

Zhang, X., Fidani, C., Huang, J., Shen, X., Zeren, Z., and Qian, J.: Burst increases of precipitating electrons recorded by the DEMETER satellite before strong earthquakes, Nat. Hazards Earth Syst. Sci., 13, 197–209, doi:10.5194/nhess-13-197-2013, 2013.

Zhang, Z., Li, X., Wu, S., Ma, Y., Shen, X., Chen, H., Wang, P., You, X., and Yuan, Y.: DEMETER satellite observations of energetic particle prior to Chile earthquake, Chinese J. Geophys., 5, 1581–1590, English version at: arXiv:1011.3592v1, 2010.

NHESSD

1, 3553–3575, 2013

Table 1. Locations of the VLF transmitters displayed in Figs. 6–8.

Call signs	Frequency (kHz)	Latitude (°)	Longitude (°)
KRA[1]	11.90	45.50	38.10
NOV[1]	12.65	55.60	84.40
KOM[1]	14.88	50.32	136.59
UBE	16.20	52.90	158.55
HWU[2]	18.30	46.70	01.23
NST	18.60	−38.48	146.93
GQD	19.60	52.91	−3.28
NWC	19.80	−21.82	114.17
HWV	20.90	48.54	02.52
NPM	21.40	21.42	−158.15
NDT	22.20	32.08	130.83
DHO	23.40	53.08	07.61
NAA	24.00	44.65	−67.29
NLK	24.80	48.20	−121.92
TBB	26.70	37.43	26.70
JJY-40	40.00	37.37	140.85
NAU	40.80	40.80	−67.18
NSY	45.90	38.00	13.50
NML	46.37	46.36	−98.34
GYW1	51.95	57.62	1.09
WWVB	60.00	40.56	−105.07
JJY-60	60.00	33.46	130.17
FUG	62.60	43.45	2.09

[1] This Russian system for long range radio navigation operates on the frequencies: 11.8, 12.6, 14.8 kHz.
[2] HWU alternates between 18.3 kHz, 21.75 kHz and 22.6 kHz, 15.1 kHz is seldom used.

NHESSD
1, 3553–3575, 2013

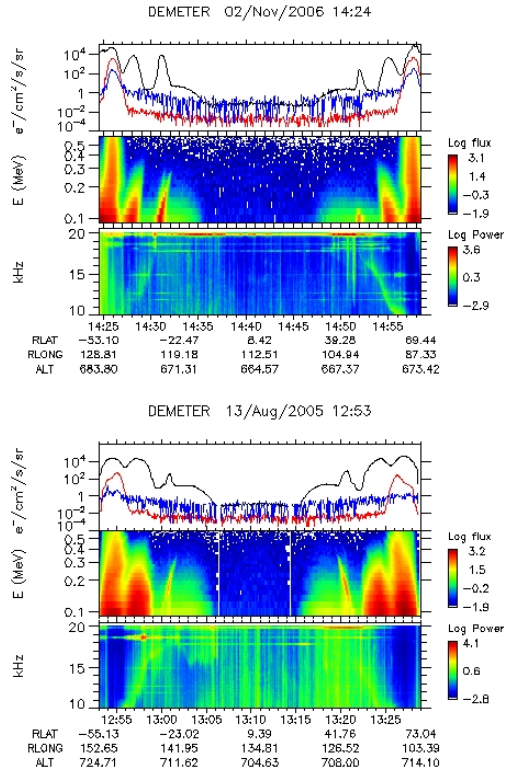

Fig. 1. (a) Energetic electrons and wave data along a half orbit on 2 November 2006. The top panel gives the variations of the electron fluxes in three energy ranges (90–526 keV, 526–971 keV and 971–2350 keV). The middle panel shows the electron energy time spectrogram and the bottom panel gives the frequency-time spectrogram of the electric component of the VLF waves in the frequency range from 10 kHz to 20 kHz. The color-coded electron flux is expressed in part/(cm^2 s ster keV) and the wave power is expressed in $\mu V^2.m^{-2}s^{-1}$. **(b)** Same as Fig. 1a for a pass on 13 August 2005.

NHESSD
1, 3553–3575, 2013

Comment on Sideropoulos et al. (2011)

J.-A. Sauvaud et al.

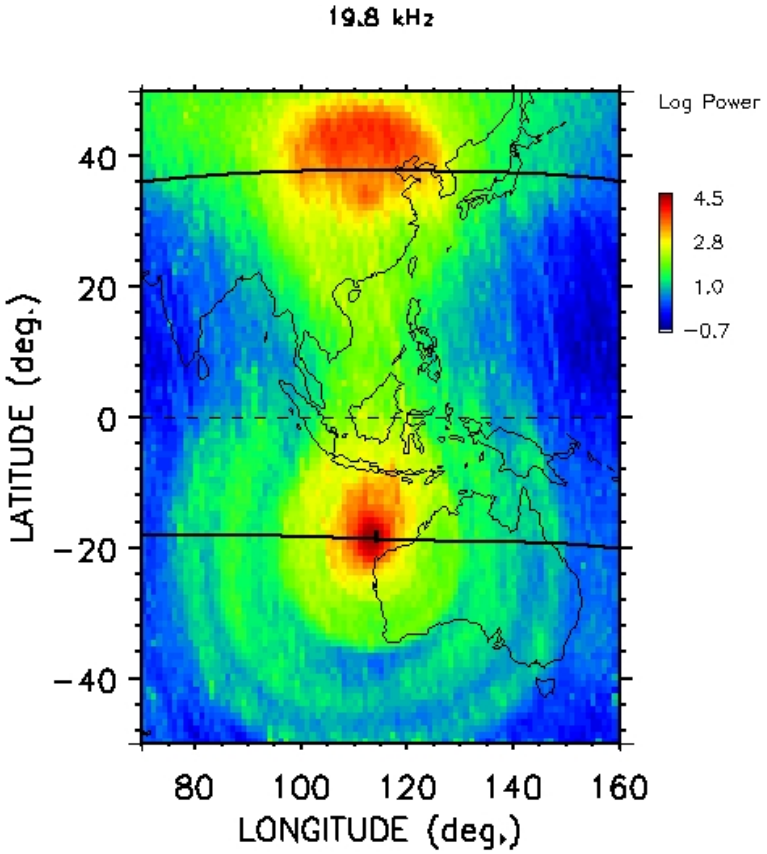

Fig. 2. Distribution of the electric power ($\mu V^2\,m^{-2}\,s^{-1}$) of the NWC transmitter at Demeter altitudes (2007–2009). The power of the NWC transmitter is 10^4 higher than that measured at 13:20 UT on 13 August 2005 in the frequency range10–19 kHz (see Fig. 1b). The black curves indicate the L = 1.4 contours at the satellite altitude.

NHESSD
1, 3553–3575, 2013

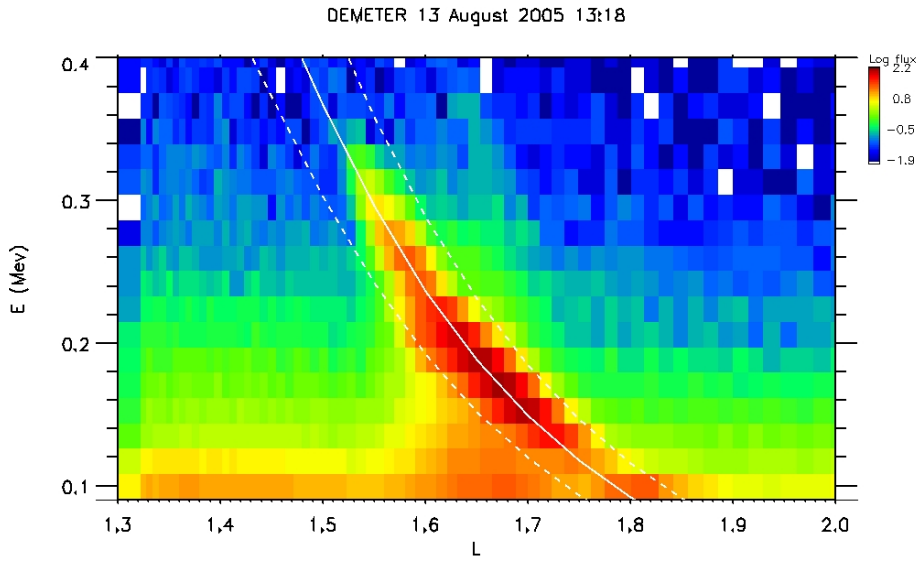

Fig. 3. Electron energy-L spectrogram for the structure recorded on 13 August 2005 starting at 13:18 UT. The white line is the result of the computation of wave-particle interaction described in the text. The dashed lines are for a plasmaspheric plasma density enhanced (lower curve) and divided by a factor 1.3 (upper curve). The color-coded electron flux is expressed in part/(cm^2 s ster keV).

NHESSD
1, 3553–3575, 2013

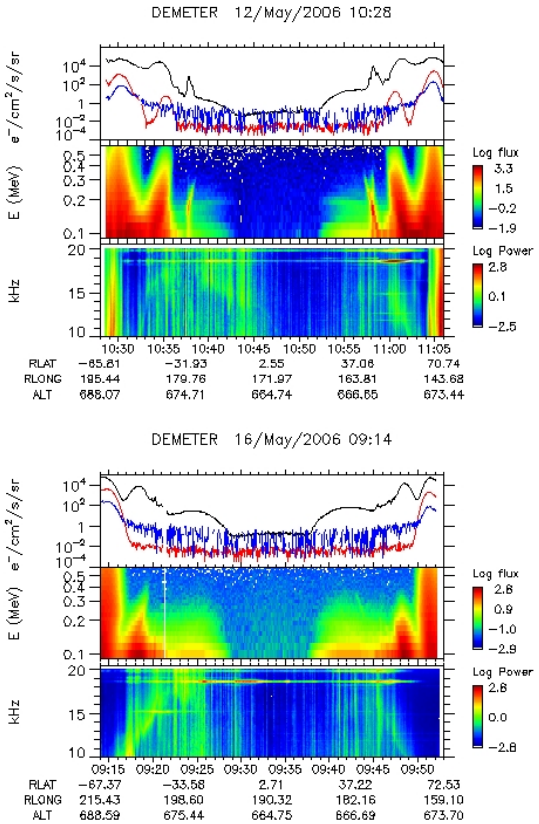

Fig. 4. (a) Electron measurements on 12 May 2006 between 10:26 UT and 11:06 UT. Conjugate electron wisps are detected around 10:38 and 10:58 UT. **(b)** Same as panel **(a)** for 16 May 2006. This Figure must be compared to Figs. 3 and 4 of Sideropoulos et al. (2011). The color-coded electron flux is expressed in part/(cm^2 s ster keV) and the wave power is expressed in $\mu V^2\,m^{-2}\,s^{-1}$.

NHESSD
1, 3553–3575, 2013

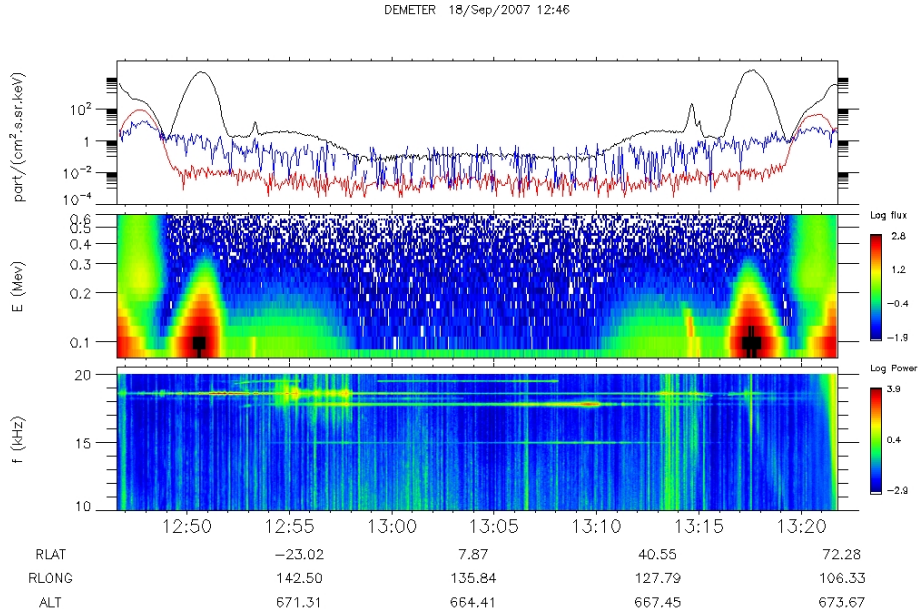

Fig. 5. Same format as Figs. 1 and 4, for 18 September 2007 between 12:46 and 13:22 UT, when NWC was off.

NHESSD
1, 3553–3575, 2013

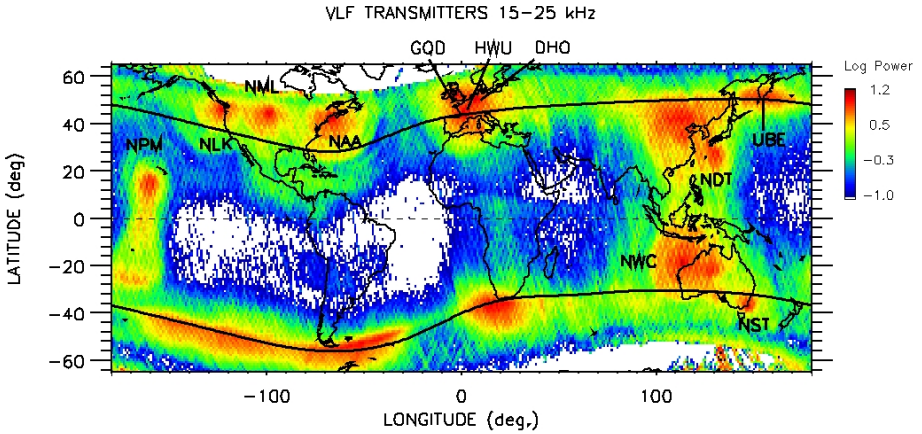

Fig. 6. Average distribution of electric power in the 15–25 kHz range measured during night passes during 3 yr (2007–2009). The corresponding transmitters are indicated by their international code. The two black lines indicate the $L = 2$ contours in the Northern and the Southern Hemisphere. The wave power is expressed in $\mu V^2\,m^{-2}\,s^{-1}$.

NHESSD
1, 3553–3575, 2013

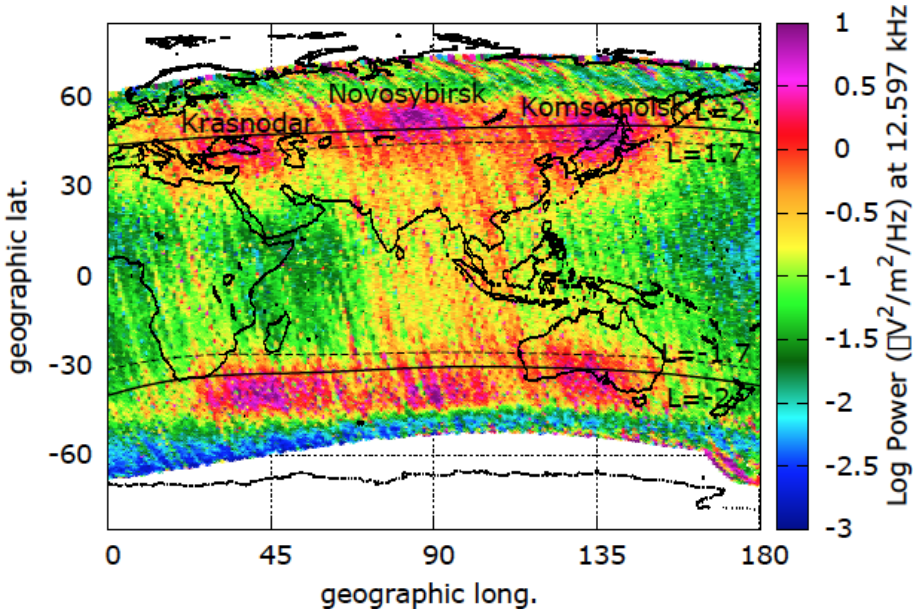

Fig. 7. Position of the three Russian transmitters emitting in the Northern Hemisphere at 11.8, 12.6 and 14.8 kHz. The wave power is expressed in $\mu V^2\,m^{-2}\,s^{-1}$.

NHESSD
1, 3553–3575, 2013

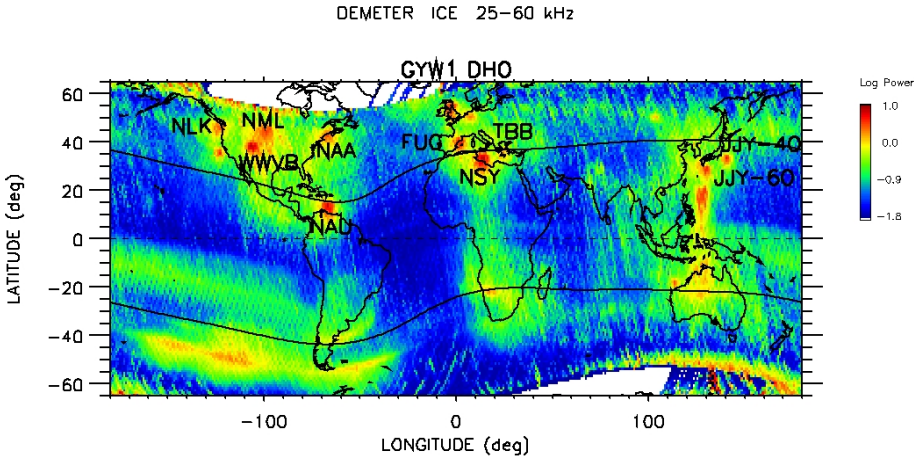

Fig. 8. Average distribution of electric power in the 25–60 kHz range measured during night passes during 3 yr (2007–2009). The corresponding transmitters are indicated by their international code. The two black lines indicate the $L = 1.5$ contours in the Northern and the Southern Hemisphere. The wave power is expressed in $\mu V^2\,m^{-2}\,s^{-1}$.

NHESSD
1, 3553–3575, 2013

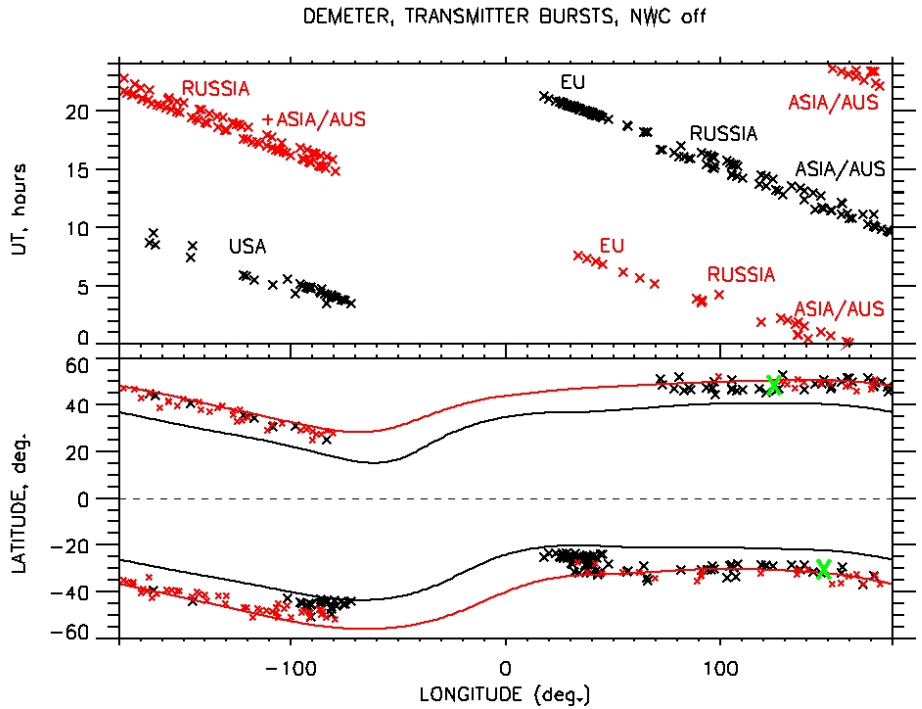

Fig. 9. UT-longitude (top) and latitude-longitude distribution of electron burst during 3 month (July, August and September 2007), when the NWC transmitter is off. The red symbols indicate measurements made around 10:00 LT while the black symbols are for 22:00 LT. The red and black curves in the bottom panel show respectively the $L = 2$ and $L = 1.5$ locations in the Northern and Southern Hemisphere. The green crosses corresponds to the measurement of electron bursts presented in Sideropoulos et al. (2011) as due to a precursor of an earthquake. The regions where the bursts are produced are indicated in the top panel.

NHESSD
1, 3553–3575, 2013

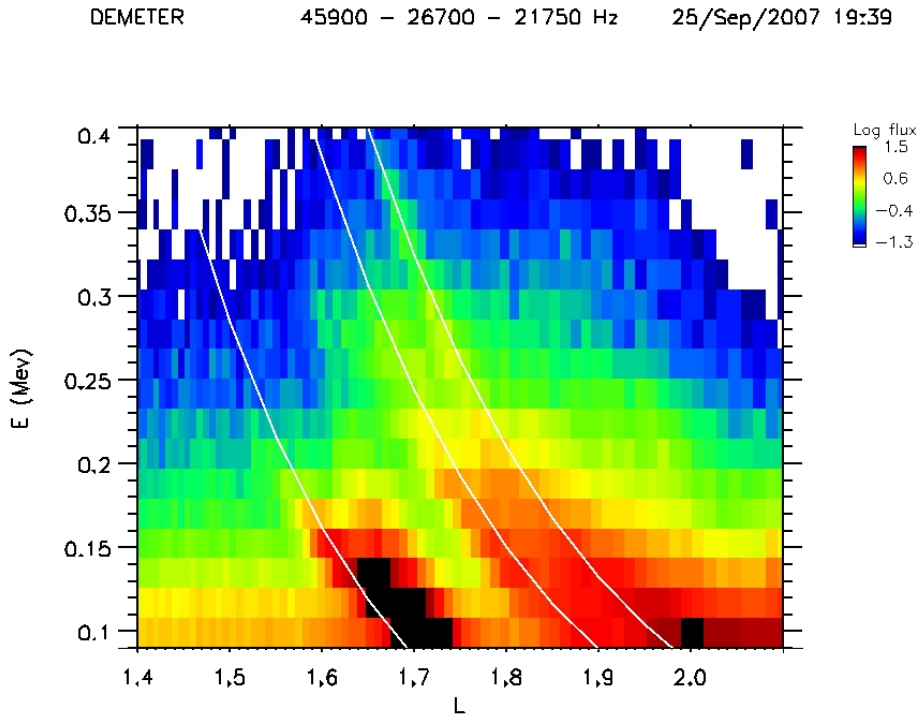

Fig. 10. Multiple electron wisps measured in the South African sector resulting from the cyclotron interaction of human VLF waves with electrons from the inner belt. Computed energy dispersion of electron resonating with monochromatic waves emitted at 45 900, 26 700 and 21 750 Hz are shown by the white curves. The color-coded electron flux is expressed in part/(cm^2 s ster keV).

NHESSD
1, 3553–3575, 2013